

Investigation of Residual Stress Distribution and Its Influence on Machining Deformation in 6061-T651 Aluminum Alloy Plates Using Crack Compliance Method

HE Wenbo¹, FAN Longxin^{2*}, YUAN Weidong³, YANG Yinfei¹, XU Jiuhoa¹

1. College of Mechanical and Electrical Engineering, Nanjing University of Aeronautics and Astronautics,

Nanjing 210016, P. R. China;

2. School of Mechanical Engineering and Rail Transit, Changzhou University, Changzhou 213164, P. R. China;

3. Nanjing Engineering Institute of Aircraft Systems AVIC, Nanjing 211106, P. R. China

(Received 29 March 2025; revised 4 June 2025; accepted 10 June 2025)

Abstract: To investigate the residual stress distribution and its influence on machining deformation in 6061-T651 aluminum alloy plates, this paper uses the crack compliance method to study the residual stress characteristics of 6061-T651 aluminum alloy plates with a thickness of 75 mm produced by two domestic manufacturers in China. The results indicate that both types of plates exhibit highly consistent and symmetrical M-shaped residual stress profile along the thickness direction, manifested as surface layer compression and core tension. The strain energy density across all specimens ranges from 1.27 kJ/m³ to 1.43 kJ/m³. Machining deformation simulations of an aerospace component incorporating these measured stresses showed minimal final deformation difference between the material sources, with a maximum deviation of only 0.009 mm across specimens. These findings provide critical data for material selection and deformation control in aerospace manufacturing.

Key words: residual stress; aluminum alloy pre-stretched plate; crack compliance method; integrated structural components; machining deformation

CLC number: V262.3

Document code: A

Article ID: 1005-1120(2025)03-0287-10

0 Introduction

Monolithic aerospace components, serving as critical load-bearing structures in aircraft, are predominantly manufactured through bulk machining of high-strength aluminum alloy thick plates. However, the dynamic release and redistribution of residual stresses during machining induce significant deformation, leading to dimensional inaccuracies, assembly challenges, and potential stress corrosion risks, thereby compromising manufacturing precision and operational reliability^[1-2]. With the ongoing national strategy for material domestication in defense equipment, the characterization of residual stress in domestic 6061-T651 aluminum alloy plates and their

engineering applicability have emerged as pressing research priorities^[3-4].

In residual stress measurement, the crack compliance method has gained prominence for aerospace aluminum alloys due to its high sensitivity, cost-effectiveness, and full-thickness characterization capability^[5]. Originally proposed by Vaidyanathan and Finnie in 1971^[6], the methodology was streamlined by Cheng and Finnie through strain gauge integration in 1986^[7-8]. Prime et al.^[9] pioneered its application to residual stress analysis in pre-stretched aluminum plates. Subsequent validation studies by Wang et al.^[10] compared crack compliance results with hole-drilling and X-ray diffraction methods for 7075 aluminum alloys. Wang et al.^[11] extended the tech-

*Corresponding author, E-mail address: fanlx@cczu.edu.cn.

How to cite this article: HE Wenbo, FAN Longxin, YUAN Weidong, et al. Investigation of residual stress distribution and its influence on machining deformation in 6061-T651 aluminum alloy plates using crack compliance method[J]. Transactions of Nanjing University of Aeronautics and Astronautics, 2025, 42(3): 287-296.

<http://dx.doi.org/10.16356/j.1005-1120.2025.03.002>

nique to thick-plate residual stress detection, while Tang et al.^[12] conducted systematic uncertainty analyses and optimization of interpolation functions. Huang et al.^[13] developed a finite element-parametric modeling framework combined with MATLAB automation to enhance residual stress profiling accuracy in 2124-T851 aluminum plates. Marco et al.^[14] addressed computational deviations through analytical formulation of integral equations using linear elastic fracture mechanics (LEFM) weight functions, effectively eliminating discretization errors.

Significant progress has been made in machining deformation prediction. Nervi et al.^[15] established a computational framework demonstrating the critical influence of geometric positioning effects on thin-walled component distortion. Fan et al.^[16] proposed a thermodynamic energy-based methodology for rapid distortion prediction, correlating residual stress fluctuations with component geometry. Huang et al.^[17] developed a strain energy-driven distortion model validated through finite element-experimental synergy. Richter et al.^[18] introduced a hybrid experimental-numerical approach for deformation prognosis in high-speed machined assemblies.

While extensive research exists on residual stress distributions in imported 2024 and 7075 aluminum alloys, systematic studies on domestic 6061-T651 thick plates remain scarce. Notably, variations in casting, rolling, and heat treatment processes across manufacturers may induce significant divergence in residual stress characteristics. The micro-scale stress state critically governs macro-scale machining behavior, necessitating quantitative analysis of stress-deformation coupling mechanisms for precision control.

This study presents the first systematic investigation into the residual stress distribution of 75-mm-thick 6061-T651 plates from Southwest Aluminum (Group) Co., Ltd. and Northeast Light Alloy Co., Ltd. The residual stress field reconstruction is achieved through crack compliance measurements. Subsequent machining deformation simulations of aerospace components quantitatively elucidate the influence mechanism of residual stress variations.

The results establish new benchmarks for domestic aluminum alloy performance evaluation while providing theoretical support for material selection, process optimization, and deformation prediction in aviation manufacturing, significantly contributing to China's autonomous high-end equipment development.

1 Principle of Crack Compliance Method

The crack compliance method reconstructs stress fields by characterizing the mechanical behavior of materials during crack propagation^[9]. When an artificial crack is introduced on the specimen surface, the residual stress release induces a characteristic displacement field across the crack flanks. In this study, a double-cutting procedure is employed: Two sequential cuts are performed on each specimen to obtain residual stresses along both the rolling direction (longitudinal) and transverse direction within the bulk material, as illustrated in Fig.1.

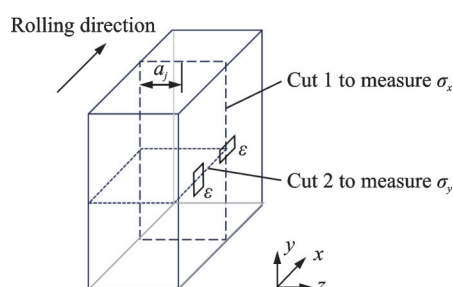


Fig.1 Schematic diagram of crack compliance method testing

Assuming the residual stress varies along the thickness direction (z -axis), its distribution can be expressed as a function of depth coordinate z using a series expansion, namely

$$\sigma_{x,y}(z) = \sum_{i=1}^n A_i P_i(z) = \mathbf{P}\mathbf{A} \quad (1)$$

where $\sigma_{x,y}(z)$ denotes the stress component (x or y direction) at depth z ; A_i the undetermined coefficients, and $P_i(z)$ the interpolation functions, typically selected as Legendre polynomials. The matrix \mathbf{P} contains basis functions, and \mathbf{A} is the coefficient vector.

To determine the coefficients A_i , the strain response at the strain gauge location (Fig.1) is calculated as a function of crack depth a_j . This response, termed the compliance function C_{ij} , is derived through theoretical analysis. By the superposition principle, the measured strain can also be expressed as a series expansion, namely

$$\epsilon_{x,y}(a_j) = \sum_{i=1}^n A_i C_i(a_j) = \mathbf{C}\mathbf{A} \quad (2)$$

where $\epsilon_{x,y}(a_j)$ denotes the measured strain (x or y direction) at crack depth a_j , and a_j the j th crack depth. The term $C_i(a_j)$ (equivalent to C_{ij}) represents the compliance function, and \mathbf{C} the compliance matrix mapping stresses to strains.

A least squares minimization is applied to reconcile the compliance-derived strains with experimental strain measurements, shown as

$$\frac{\partial}{\partial A_i} \sum_{j=1}^m \left[\epsilon_{\text{measured}}(a_j) - \sum_{k=1}^n A_k C_k(a_j, P_k) \right]^2 = 0 \quad (3)$$

$i = 1, 2, \dots, n$

where m denotes the number of strain measurements, with $m \geq n$ in practice, and j is the measurement index. $\epsilon_{\text{measured}}(a_j)$ indicates the experimentally measured strain at depth a_j , while k is a dummy summation index. The compliance function $C_k(a_j, P_k)$ explicitly shows dependence on basis function P_k .

$$\mathbf{A} = (\mathbf{C}^T \mathbf{C})^{-1} \mathbf{C}^T \epsilon_{\text{measured}} = \mathbf{B} \epsilon_{\text{measured}} \quad (4)$$

where \mathbf{B} denotes the least-squares solution matrix $\mathbf{B} = (\mathbf{C}^T \mathbf{C})^{-1} \mathbf{C}^T$.

2 Wire Cutting Experiment

2.1 Specimen preparation

This study employed two domestically produced 6061-T651 aluminum alloy pre-stretched plates from different manufacturers, both with a thickness of 75 mm. The T651 temper designation indicates that the material underwent stress relief prior to artificial aging, distinguishing it from the T6 temper where artificial aging is performed directly after quenching. Specimens were extracted from two source plates: A 3 000 mm × 225 mm × 75 mm

plate produced by Northeast Light Alloy Co., Ltd., and a 3 660 mm × 1 525 mm × 75 mm plate manufactured by Southwest Aluminum Co., Ltd. These specimens were utilized to investigate the residual stress distribution along both the rolling direction (RD) and transverse direction (TD) of the aluminum alloy plates. The geometric specifications of the prepared specimens are summarized in Table 1.

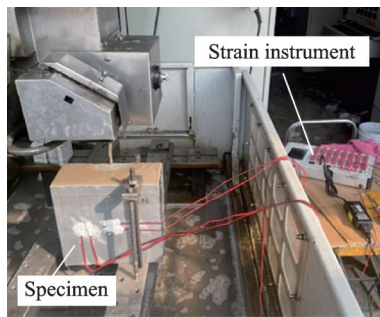
Table 1 Specimen specifications

No.	Dimension/ (mm × mm × mm)	Manufacturer
1	170 × 170 × 75	Southwest Aluminum Industry
2	170 × 170 × 75	Southwest Aluminum Industry
3	170 × 170 × 75	Northeast Light Alloy
4	170 × 170 × 75	Northeast Light Alloy

2.2 Electrical discharge wire cutting

The specimen cracks were introduced using electrical discharge wire cutting technology, performed on an EFH54S CNC wire-cutting machine tool manufactured by Shanghai Yiyang. The cutting parameters included a discharge current of 3 A, wire feed speed of 3 m/s, and cutting feed rate of 5 mm/min, with deionized water employed as the coolant. A 0.18 mm diameter molybdenum wire was utilized as the electrode, producing a final crack width of approximately 0.25 mm. The medium-speed wire-cutting offers a balance between precision and cutting efficiency, which is critical for minimizing thermal and mechanical effects during strain-relief slotting. Furthermore, the chosen parameters (current and speed) were based on a compromise between cut surface quality and avoiding secondary stress induction. BF120-3AA foil-type modified phenolic resin strain gauges with a 3.0 mm gauge length and sensitivity coefficient of $2.0 \pm 1\%$ were selected for strain measurement.

Fig.2 illustrates the experimental setup of the wire-cutting process. To protect the strain gauges from coolant damage, a protective layer of 704 silicone rubber was applied to their surfaces. Two strain gauges were simultaneously bonded at each measurement point, with readings acquired using a JM3816D static strain indicator. The arithmetic



(a) First cut of Specimen 1



(b) Second cut of Specimen 1

Fig.2 Wire cutting experiment

mean of dual measurements was adopted for data processing. The cutting procedure involved incremental depth increases of 1 mm per cutting cycle, followed by stabilization periods prior to strain recording. This iterative process continued until reaching the target depth of 45 mm. A quarter-bridge circuit configuration was implemented with temperature compensation achieved through a compensation block matching the specimen's material and dimensions.

The averaged strain measurements from two identical specimens are presented in Fig.3, demonstrating the strain evolution during progressive cutting.

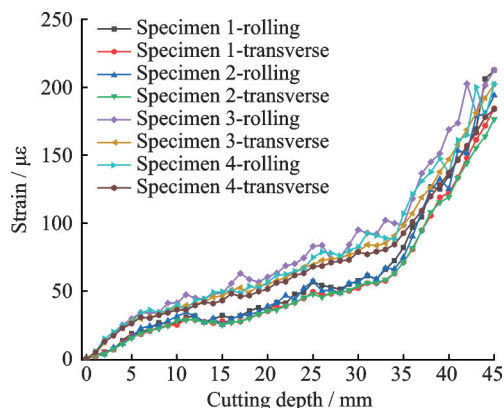


Fig.3 Average measured strain

3 Finite Element Modeling and Computation

3.1 Model establishment

This study employed ABAQUS 2021 finite element software for modeling and computing the crack compliance function matrix C . Leveraging the geometric symmetry of the specimen, only half of the specimen was modeled and meshed with the wire-cut crack as the symmetry axis, as illustrated in Fig.4. The domain was discretized using 8-node plane strain elements (CPE8). The mesh size on the left side of the specimen (adjacent to the crack) was set to half the crack width (0.125 mm, based on a nominal crack width of 0.25 mm), while the remaining regions adopted a graded mesh transitioning from 0.125 mm to 2 mm from left to right. Boundary conditions were defined as follows: The x -direction displacement on the left edge of the specimen and both x - and z -direction displacements at the bottom-left corner node were fully constrained. The material properties assigned to the model included an elastic modulus of 68 900 MPa and a Poisson's ratio of 0.33^[19].

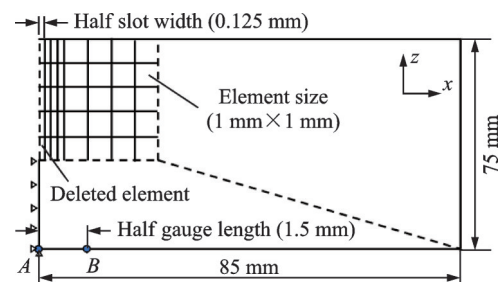


Fig.4 Schematic diagram of finite element mesh and boundary condition

3.2 Calculation of crack compliance functions

Following model construction, the 2nd to 14th order Legendre polynomials $P(z)$ were used as initial stress loads along the thickness direction of the plate. The crack propagation process was simulated by gradually removing elements in the crack region using the "Model Change" functionality. During this procedure, displacement values U_B at the strain gauge locations were recorded. The corresponding strain values were subsequently calculated according

to Eq.(5), thereby obtaining the 2nd to 14th order crack compliance functions, as illustrated in Fig.5.

$$C_{ij} = 2U_B / L_{\text{gauge}} \quad (5)$$

where L_{gauge} denotes the length of strain gauges.

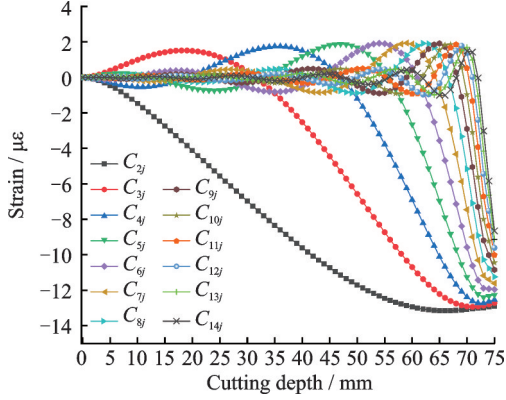


Fig.5 Crack compliance functions of specimens

3.3 Uncertainty evaluation

The uncertainty in residual stress calculations using the crack compliance method primarily originates from two sources: Strain measurement errors and model errors^[20]. Strain measurement uncertainty $s_{\epsilon,j}$ arises from random errors in strain data acquisition, representing the deviation between the least-squares-fitted strain values and experimental measurements, namely

$$s_{\epsilon,j}^2 = \text{diag}(PVP^T) = \text{diag}(PB \text{diag}(s_{\epsilon,j}^2)B^T P^T) \quad (6)$$

where $s_{\epsilon,j}^2$ denotes the strain measurement error at a crack depth $z=a_j$ and V the covariance matrix.

Model errors stem from discrepancies between the selected interpolation functions and the actual stress distribution in the plate. For a given interpolation function, the polynomial order n dominates the model-induced uncertainty. The stress uncertainty due to model error $s_{\text{model},j}$ is approximated as

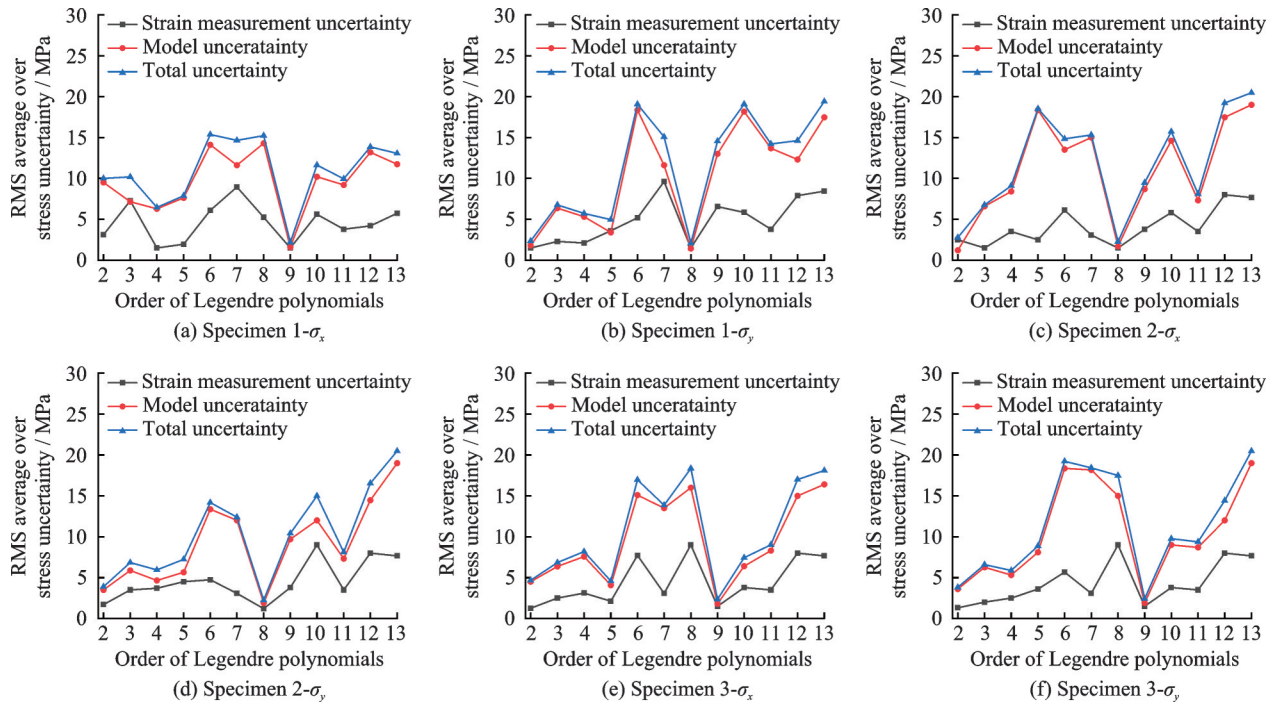
$$s_{\text{model},j}(n) \approx \frac{1}{N-1} \sum_{k=a}^b [\sigma_j(n=k) - \bar{\sigma}_j]^2 \quad (7)$$

where $\bar{\sigma}_j$ represents the mean stress over the polynomial order range $n(a-b)$, and $N=b-a+1$ the number of stress solutions. To model the uncertainty as a function of n , this study adopts $a=n-1$ and $b=n+1$.

The total uncertainty in residual stress calculation $S_{\text{total},j}$ is then

$$S_{\text{total},j} = \sqrt{S_{\epsilon,j}^2 + S_{\text{model},j}^2} \quad (8)$$

In MATLAB R2022b, Eqs.(6—8) were implemented to compute stress uncertainties at each depth layer for varying polynomial orders. Root mean square (RMS) values of these uncertainties are plotted in Fig.6. Results demonstrate significant sensitivity of uncertainty to polynomial order. For Specimen 1- σ_y , Specimen 2- σ_x , and Specimen 2- σ_y , the 8th-order Legendre polynomial minimizes total uncertainty to 2.06, 2.26, and 2.24 MPa, respectively.



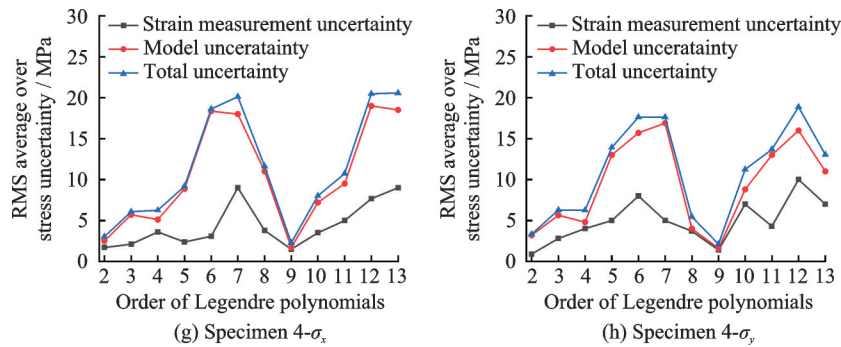


Fig.6 RMS average over stress uncertainty for different expansion orders

tively. Conversely, the 9th-order polynomials yield minimal uncertainties for other specimens. Consequently, the 8th-order Legendre polynomials were selected for Specimen 1- σ_y , Specimen 2- σ_x , and Specimen 2- σ_y , while the 9th-order polynomials were applied to remaining stress components.

4 Experimental Results and Discussion

4.1 Residual stress measurement results

The residual stress distributions and their total uncertainties for two aluminum alloy pre-stretched plates were calculated using MATLAB 2022b software, based on the residual stress formulation and the optimal order of Legendre polynomials. The results are presented in Fig.7. Also, the comparison of the maximum compressive and tensile stresses values of four specimens are shown in Table 2. As illustrated in Fig.7, the residual stress curves along the thickness direction exhibit similar trends in both RD and TD, demonstrating a distinct M-shaped distribution pattern. The residual stresses are symmetrically distributed about the mid-plane of the plate and approach zero at the mid-plane. The average re-

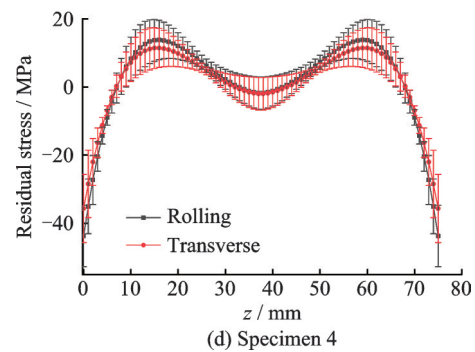
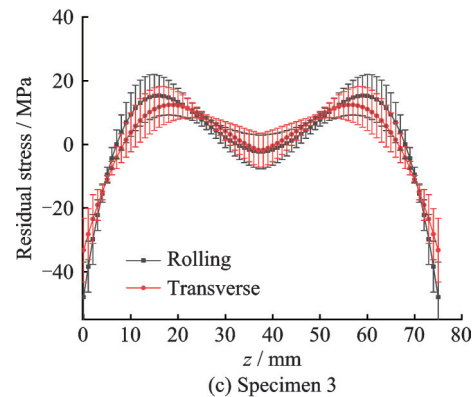
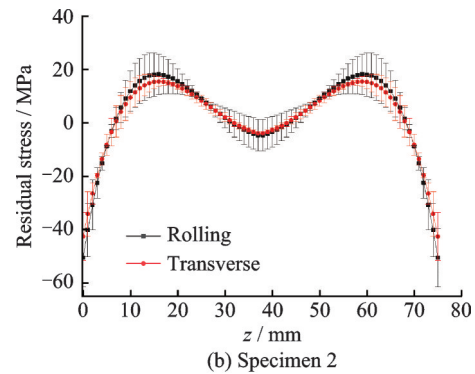
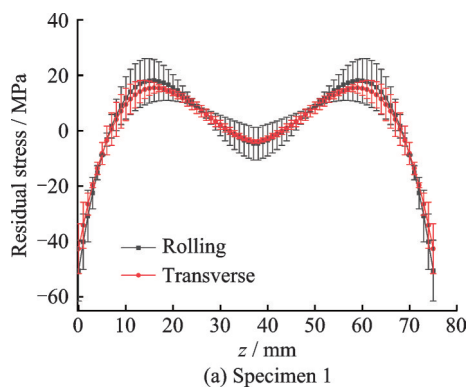


Fig.7 Residual stress profiles

sidual stress in the TD is approximately 70% of that in the RD. In both directions, the maximum residual compressive stresses occur near the plate surfaces, reaching approximately -50 MPa in the RD and -42 MPa in the TD. Conversely, the peak tensile residual stresses are not located at the mid-plane

Table 2 Comparison of the residual stress values of four specimens

No.	Maximum compressive stress/MPa		Maximum tensile stress/MPa	
	RD	TD	RD	TD
1	−50.5	−42.6	18.1	15.4
2	−37.4	−29.5	14.5	11.2
3	−48.0	−33.2	15.3	12.4
4	−43.7	−35.6	13.8	11.4

but at approximately 15 mm beneath the surface, with maximum values of 18.6 MPa in the RD and 15.7 MPa in the TD. A severe plastic deformation layer, induced by rolling, quenching, and stretching processes, exists within 1–2 mm of the surface, where stress fluctuations reach ± 17 MPa. Across all specimens, the residual stresses fluctuate within a range of -50 MPa to 20 MPa throughout the plate thickness. Although the residual stress magnitudes in the aluminum alloy pre-stretched plates are relatively low, the crack compliance method effectively characterizes the distribution patterns of these residual stresses.

4.2 Residual stress evaluation based on strain energy density

Regarding the detrimental effects of residual stress on machining deformation, strain energy density serves as an effective indicator for evaluating global stress distribution. The strain energy density reveals the global stress state of the blank, and its application in blank assessment enables characterization of deformation risks in post-machined components. By considering anisotropic material properties, more precise results can be obtained. In this context, the strain energy densities along the rolling direction and transverse direction are respectively expressed as

$$u_x = \frac{1}{t} \int_0^t \frac{\sigma_x^2 - \nu \sigma_x \sigma_y}{2E} dz \quad (9)$$

$$u_y = \frac{1}{t} \int_0^t \frac{\sigma_y^2 - \nu \sigma_x \sigma_y}{2E} dz \quad (10)$$

where t denotes the blank thickness, E the elastic modulus, and ν the Poisson's ratio. The stress distribution along the rolling direction is designated as

σ_x , and σ_y corresponds to the transverse direction. The total strain energy density of the material is defined as the summation of strain energy densities in both orthogonal directions, $u = u_x + u_y$.

The relationship between strain energy density and deformation risk is shown in Fig.8. When the total energy density of the blank is less than 1 kJ/m^3 , it can be expected that there is no significant risk of deformation in the final part. When the total energy density is greater than 2 kJ/m^3 , there will be a significant risk of deformation of the parts. When the total energy density is between 1 kJ/m^3 and 2 kJ/m^3 , there is a possible risk of deformation of the part, and the deformation of the part is also closely related to its geometric structure^[21].

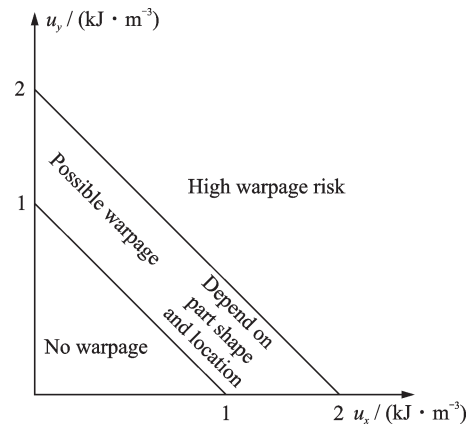


Fig.8 Relationship between strain energy density and deformation risk

Based on the measured initial residual stress distribution of the blank, a strain energy density analysis was performed for the four measured stress distributions. The strain energy densities in the rolling direction, transverse direction, and the total strain energy density were calculated respectively, with the results summarized in Table 3. As shown in Table 3, the calculated total strain energy densities for all four tested specimen blanks fall within the range of $1\text{--}2 \text{ kJ/m}^3$, suggesting possible deformation risks in the final components. Consequently, judicious selection of processing parameters during engineering applications is imperative to mitigate out-of-tolerance risks.

Table 3 Strain energy density of specimens

No.	$u_x/(\text{kJ}\cdot\text{m}^{-3})$	$u_y/(\text{kJ}\cdot\text{m}^{-3})$	$u/(\text{kJ}\cdot\text{m}^{-3})$
1	0.74	0.53	1.27
2	0.73	0.59	1.32
3	0.78	0.65	1.43
4	0.71	0.58	1.29

4.3 Deformation analysis of typical structural machining

To investigate the influence of residual stress variations in materials from different manufacturers on component deformation, a typical aeronautical monolithic structural component was designed. The geometry and dimensions of the component are illustrated in Fig.9. The blank dimensions measure $905\text{ mm}\times 400\text{ mm}\times 75\text{ mm}$. A finite element simulation method was employed to simulate the material removal process and analyze the final deformation of the component induced by residual stresses within the blank.

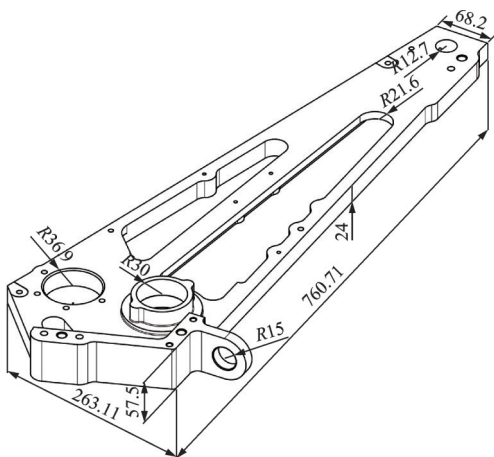


Fig.9 Schematic diagram of parts

A model identical in dimensional specifications to both the blank and the designed part was established in ABAQUS, with the initial residual stress distribution from Fig.7 applied as the initial stress condition. Fig.10(a) illustrates the designed geometry of the blank containing initial residual stresses. The model was meshed using C3D10 elements, comprising 220 980 elements and 312 453 nodes. The element “birth and death” technique was employed to simulate material removal processes. As this study focuses exclusively on comparative analy-

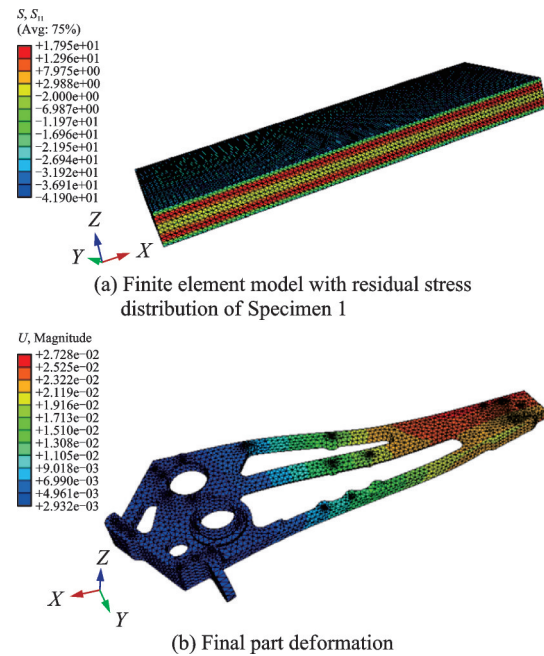


Fig.10 Finite element simulation process

sis of final part deformations, all machinable material was removed in a single analysis step. Fig.10(b) presents the final deformation results with residual stress distribution of Specimen 1.

The deformation behavior of components induced by four distinct residual stress distributions was analyzed through simulation, with the maximum deformation values extracted and compared, as illustrated in Fig.11. The final deformation measurements for the four specimens exhibited minimal magnitudes of 0.027, 0.018, 0.022, and 0.026 mm, respectively. Notably, these deformation values demonstrate close agreement with a maximum deviation of merely 0.009 mm. This narrow variation range substantiates the high degree of consistency in residual stress distributions among products from

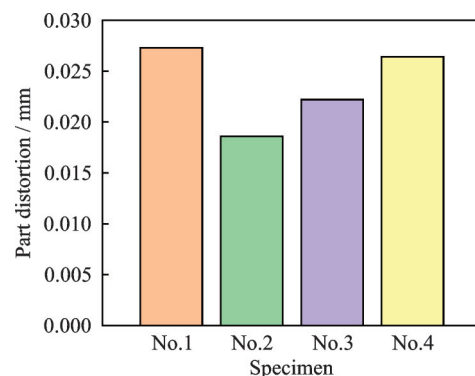


Fig.11 Maximum final deformation of different specimens

different manufacturers within the scope of this investigation.

5 Conclusions

(1) Residual stress measurements using the crack compliance method on 75 mm-thick domestic 6061-T651 plates revealed a consistent M-shaped profile through the thickness for both the RD and TD. The average TD residual stress was approximately 70% of the RD value.

(2) In both RD and TD, the maximum residual compressive stresses are near the plate surfaces, reaching about -50.2 MPa in RD and -42 MPa in TD. Peak tensile residual stresses are around 15 mm beneath the surface, measuring 18.6 MPa in RD and 15.7 MPa in TD.

(3) The total strain energy density of all four tested specimens is in the range of $1\text{--}2$ kJ/m³, signaling potential machining-induced deformation risks, while actual part deformation also largely depends on component geometry.

(4) Machining deformation simulations of a representative aerospace component showed minimal differences between manufacturers. The maximum deformation deviation across specimens was only 0.009 mm, confirming high consistency in residual stress distributions.

References

- [1] EL-ATY A A, XU Y, GUO X, et al. Strengthening mechanisms, deformation behavior, and anisotropic mechanical properties of Al-Li alloys: A review[J]. *Journal of Advanced Research*, 2018, 10(C): 49-67.
- [2] CHEN J S, LIU C Q, ZHAO Z W, et al. Inference method for residual stress field of titanium alloy parts based on latent Gaussian process introducing theoretical prior[J]. *Transactions of Nanjing University of Aeronautics and Astronautics*, 2024, 41(2): 135-146.
- [3] ZHAO Yaobang, CHEN Bo, WANG Jianfeng, et al. Research on difference of residual stress in friction stir welding between multi-segment and long-segment cylindrical shell[J]. *Journal of Nanjing University of Aeronautics & Astronautics(Natural Science Edition)*, 2025, 57(1): 92-99. (in Chinese)
- [4] LI W, MA L, WAN M, et al. Modeling and simulation of machining distortion of pre-bent aluminum alloy plate[J]. *Journal of Materials Processing Technology*, 2018, 258: 189-199.
- [5] GUO J, FU H, PAN B, et al. Recent progress of residual stress measurement methods: A review[J]. *Chinese Journal of Aeronautics*, 2021, 34(2): 54-78.
- [6] VAIDYANATHAN S, FINNIE L. Determination of residual stresses from stress intensity factor measurements[J]. *Journal of Basic Engineering*, 1971 (93): 242-246.
- [7] CHENG W, FINNIE L. Measurement of residual hoop stress in cylinders using the compliance method [J]. *Journal of Engineering Materials and Technology*, 1986(108): 87-92.
- [8] CHENG W, FINNIE L. The crack compliance method for residual stresses measurement[J]. *Welding in the World*, 1990(28): 103-110.
- [9] PRIME M B, HILL M R. Residual stress, stress relief, and inhomogeneity in aluminum plate[J]. *Scripta Materialia*, 2002, 46(1): 77-82.
- [10] WANG Qiucheng, KE Yinglin, ZHANG Qiaofang. Evaluation of residual stress depth profiling in 7075 aluminum alloy plates[J]. *Acta Aeronautica et Astronautica Sinica*, 2003, 24(4): 336-338. (in Chinese)
- [11] WANG S H, ZUO D W, WANG M, et al. Modified layer removal method for measurement of residual stress distribution in thick pre-stretched aluminum plate[J]. *Transactions of Nanjing University of Aeronautics and Astronautics*, 2004, 21(4): 286-290.
- [12] TANG Z T, LIU Z Q, AI X, et al. Measuring residual stresses depth profile in pre-stretched aluminum alloy plate using crack compliance method[J]. *Chinese Journal of Nonferrous Metals*, 2007, 17(9): 1404-1409.
- [13] HUANG X, SUN J, ZHOU C A, et al. Development of simulation system for compliance function and residual stress measurement for Al 2124-T851 plate[J]. *Procedia CIRP*, 2016, 57: 591-594.
- [14] MARCO B, TOMMASO G. Measuring residual stresses with crack compliance methods: An ill-posed inverse problem with a closed-form kernel[J]. *Applied Mechanics*, 2024, 5(3): 475-489.
- [15] NERVI S, SZABÓ B A, YOUNG K A. Prediction of distortion of airframe components made from aluminum plates[J]. *AIAA Journal*, 2009, 47(7): 1635-1641.
- [16] FAN L X, TIAN H, LI L, et al. Machining distortion minimization of monolithic aircraft parts based on the energy principle[J]. *Metals*, 2020, 10(12): 1586.
- [17] HUANG X M, SUN J, LI J F. Mathematical modeling of aeronautical monolithic component machining

- distortion based on stiffness and residual stress evolution[J]. Chinese Journal of Mechanical Engineering, 2017, 53(9): 201-208.
- [18] RICHTER T V, KOCH D, WITTE A, et al. Methodology for prediction of distortion of workpieces manufactured by high speed machining based on an accurate through-the-thickness residual stress determination[J]. The International Journal of Advanced Manufacturing Technology, 2013, 68(9): 2271-2281.
- [19] FRUTOS J A, AMBRIZ R R, GARCIA C J, et al. Orthogonal impact load in 6061-T651 and 7075-T651 aluminum alloy plates[J]. Journal of Materials Research and Technology, 2023, 26: 4245-4262.
- [20] OLSON M D, DEWALD A T, HILL M R. Precision of hole-drilling residual stress depth profile measurements and an updated uncertainty estimator[J]. Experimental Mechanics, 2021, 61: 549-564.
- [21] LEQUEU P, LASSINCE P, WARNER T, et al. Engineering for the future: Weight saving and cost reduction initiatives[J]. Aircraft Engineering & Aerospace Technology, 2001, 73(2): 147-159.

Acknowledgements This work was supported in part by the National Natural Science Foundation of China (Nos. 61201048, 61107063), and the National Science and Technology Major Project (No.2017-VI-001-0094).

Authors

The first author Mr. HE Wenbo is currently a doctoral

student majoring in mechanical manufacturing and automation at Nanjing University of Aeronautics and Astronautics. His research focuses on deformation control technology for efficient and precise machining of aviation structural components, as well as the design of flexible fixtures for efficient machining, etc.

The corresponding author Dr. FAN Longxin received the Ph.D. degree in mechanical engineering in Nanjing University of Aeronautics and Astronautics, Nanjing, China, in 2021. He is currently a lecture in School of Mechanical Engineering and Rail Transit in Changzhou University. His research has focused on basic and applied research on precision cutting technology for integral structural components, cutting of difficult to machine materials, etc.

Author contributions Mr. HE Wenbo designed the study, compiled the models, conducted the analysis, interpreted the results and wrote the manuscript. Dr. FAN Longxin contributed to algorithm development, supported the analysis, and revised the manuscript. Dr. YUAN Weidong contributed to data and material for the stress measurement experiment. Prof. YANG Yinfei and Prof. XU Jiuhua contributed to the discussion and background of the study. All authors commented on the manuscript draft and approved the submission.

Competing interests The authors declare no competing interests.

(Production Editor: SUN Jing)

基于裂纹柔度法的6061-T651铝合金板材残余应力分布研究 及其对加工变形的影响

何文博¹, 樊龙欣², 袁维东³, 杨吟飞¹, 徐九华¹

(1.南京航空航天大学机电学院,南京 210016,中国; 2.常州大学机械与轨道交通学院,常州 213164,中国;
3.航空工业南京机电液压工程研究中心,南京 211106,中国)

摘要:为探究6061-T651铝合金板材残余应力分布及其对加工变形的影响,采用裂纹柔度法研究了中国国内两家制造商生产的厚度为75 mm的6061-T651铝合金板材的残余应力特性。结果表明,两种板材均呈现高度一致、沿厚度方向对称的“M”形残余应力分布特征,表现为表面层受压、芯部受拉。所有试样的应变能密度范围为1.27 kJ/m³至1.43 kJ/m³。基于实测残余应力进行的航空整体结构件加工变形仿真显示,不同来源材料导致的最终变形差异极小,试样间最大偏差仅为0.009 mm。本文研究结果为航空航天制造中的材料选择和变形控制提供了参考数据。

关键词:残余应力;铝合金预拉伸板;裂纹柔度法;整体结构件;加工变形